ACS Photonics

pubs.acs.org/journal/apchd5

Article

Enhanced Electro-Optic Modulation in Resonant Metasurfaces of Lithium Niobate

Helena Weigand,*,† Viola V. Vogler-Neuling,† Marc Reig Escalé, David Pohl, Felix U. Richter, Artemios Karvounis, Flavia Timpu, and Rachel Grange

Cite This: https://doi.org/10.1021/acsphotonics.1c00935

Read Online

ACCESS | Metrics & More | Article Recommendations | Supporting Information

ABSTRACT: In display technologies or data processing, planar and subwavelength free-space components suited for flat photonic devices are needed. Metasurfaces, which shape the optical wavefront within hundreds of nanometers, can provide a solution for thin and portable photonic devices, for example, as CMOS-compatible modules. While conventional electro-optic modulators are inconvenient to operate in free space configurations, its principle can largely be applied to the development of active metasurfaces with the prospect of modulation speeds up to the GHz region. We extend this principle of the linear electro-optic effect to a metasurface in lithium niobate with an optical resonance in the visible. We exploit the electric and optical field overlap inside the metasurface to enhance the light matter interaction. Hence, the modulation of the transmitted light is increased by 2 orders of magnitude, namely, by a factor of 80, compared to the unstructured substrate. Furthermore, we investigate the influence of the dispersive optical resonance on the wavelength-dependence of the modulation and achieve fast and continuous modulation of light at low voltage and MHz speed. This proof-of-concept work is a first important step toward the use of lithium niobate resonant nanostructures for free space modulation.

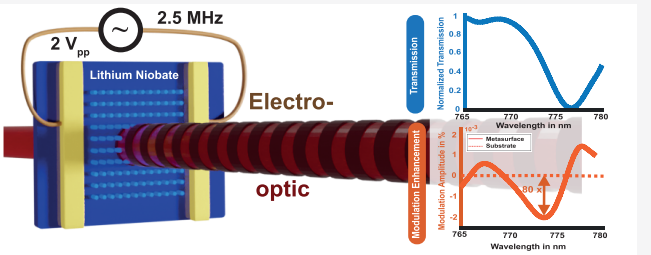

KEYWORDS: *metasurface, electro-optic, lithium niobate, modulation, enhancement, visible spectrum*

Typical photonic free space applications rely on optical elements such as lenses or polarizers with a thickness of several millimeters. A successful approach for thinner elements is metasurfaces, which influence the electromagnetic wavefront by subwavelength geometries. Although several optical operations have been achieved with metasurfaces,[1−3] a current bottleneck in the application is the tunability of their functionality. This issue is tackled by the field of active metasurfaces,[4,5] which is based either on tuning the material properties, the unit cell, or the surrounding medium. Several approaches were demonstrated by exploiting the thermo-optic effect,[6,7] nonlinear properties,[8−10] stretching,[11,12] MEMS,[13] liquid crystals,[14] plasmonics,[15−17] or phase change materials.[18,19] Tuning via electrical actuation reaches the MHz-range and includes approaches such as carrier doping, phase transition, electromechanical, or capacitance tuning.[20] Among these, the electro-optic modulation of the refractive index is one of the fastest effects,[21] which is extensively exploited for conventional modulators. Though, light intensity modulation by the linear electro-optic effect has so far not been demonstrated in an all-dielectric metasurface.

LN is an optically transparent, dielectric material widely used in electro-optic modulators,[22−24] due to its high refractive index in the visible range (n_o = 2.26 at 765 nm),[25] its high electro-optic coefficient (r_{33} = 34 pm/V),[26] and its robustness as an inorganic metal-oxide. Recently, lithium niobate metasurfaces were demonstrated, and their ability to enhance the second harmonic generation as well as spontaneous parametric-down conversion was shown.[27−30]

The electro-optic effect was realized in a metasurface in LN, but it was limited to a phase modulation at 633 nm with 300 V_{pp} and a electrode gap separation of 10 μm at 1 MHz driving frequency.[31] While the Pockels effect is an inherent LN property, here we achieve a wavelength-dependent and 80× enhanced electro-optic response around the optical resonance of the LN metasurface compared to the substrate. This active electro-optic tuning changes the intensity transmission properties and works up to MHz speeds by applying AC voltages starting from less than 1 V peak-to-peak (V_{pp}).

We choose an x-cut LN thin-film (500 nm) on top of a 2 μm silicon dioxide buffer layer and a LN substrate (Figure 1a). By top-down fabrication, we structure the film into metasurfaces with a period of 500 nm formed of pillar-shaped unit cells. The

Received: June 23, 2021

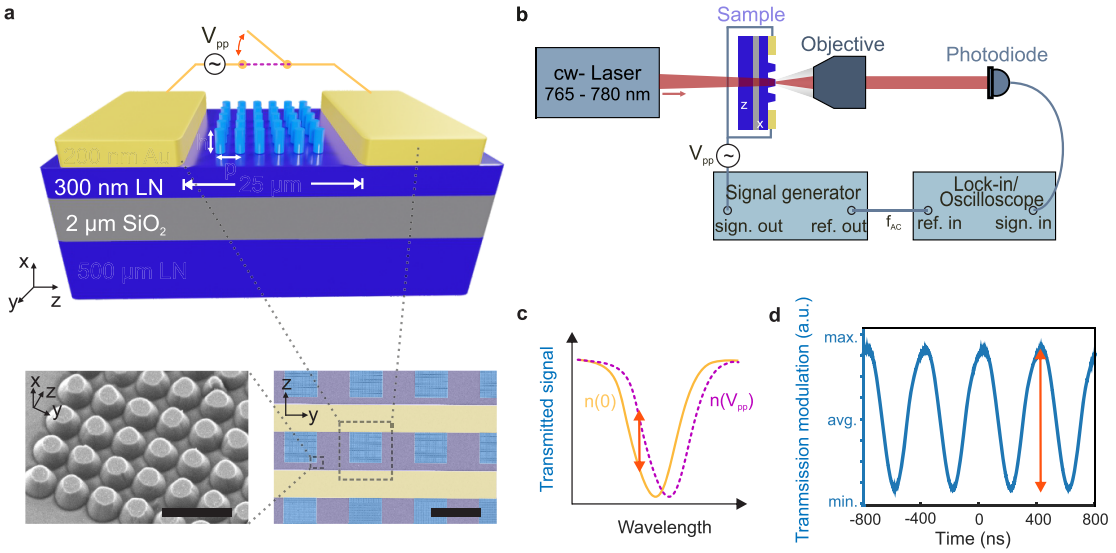

Figure 1. Design and characterization of an electro-optic metasurface. (a) Metasurface (blue LN pillars, to differentiate from the remaining LN layer) with pillars of height h and a period p between Au electrodes on top of the sample stack. The lower left inset shows the SEM image of the metasurface pillars structure. Scale bar 1 μm. The lower right inset shows a false-color SEM of several metasurfaces (purple) between the electrodes (yellow). Scale bar 30 μm. (b) Schematic of the measurement setup. (c) Schematic transmission curve (yellow line) shifted upon application of a voltage (purple line). The orange arrow marks the change of transmitted intensity, that is, the modulation amplitude. (d) Measured time trace of the transmitted intensity modulation at 772.4 nm, 22 mW laser power, 2.5 MHz voltage signal, and 10 V_{pp}.

pillars have heights of 200 nm and top radii of 89, 113, 135, and 154 nm for four different metasurfaces. A 300 nm unetched LN layer remains below the pillars. The overall size of a metasurface is 20 × 20 μm^2. Two gold electrodes with a height of 300 nm, separated by a distance of 25 μm, are used to drive the metasurfaces. The electrodes create an electric field along the r_{33} component of the LN electro-optic tensor (extraordinary z-axis, Figure 1a).[32]

Linearly polarized light from a tunable continuous wave laser, oriented perpendicular to the electrodes, that is, along the r_{33} direction of lithium niobate, probes the optical behavior of the metasurface with ∼0.5 mW optical power. To measure the electro-optic modulation, we apply an AC voltage and monitor the change in transmitted intensity through the metasurface with a lock-in amplifier or an oscilloscope (Figure 1b and SI, Figure S1). Due to the linear electro-optic effect, the voltage induces a change in the refractive index of LN, which shifts the metasurface resonance, as illustrated schematically in Figure 1c. In contrast to, for example, metalenses,[33] the intensity modulation does not require a spatially discrete phase modulation from 0 to 2π of the transmitted light but relies solely on the shift of the resonance based on the refractive index change. The AC voltage modulates the intensity of the transmitted light with the same frequency (Figure 1d). In this study, we detect this change of transmitted intensity, indicated schematically with an orange arrow with a height named modulation amplitude. We are able to track this electro-optic response using an oscilloscope and report a modulation of the transmitted intensity of 0.01% for a 180 kHz driving signal with 10 V_{pp}. This simple configuration illustrates the broad application range of our device for detection with conventional photodiodes and oscilloscopes compared to, for example, phase modulation.[33]

We determine the resonance position of the metasurface by sweeping the laser between 765 and 780 nm and measuring the transmission intensity with a silicon photodiode with a spectral resolution of 3 pm (Figure 1b). In Figure 2a, we show the measured transmission (left axis, solid blue line) of the metasurface with the steepest spectral feature of the four investigated metasurfaces in the given laser range (135 nm pillar radius), normalized to an unpatterned reference area. We observe an optical resonance with a quality factor of 129 at 776.6 nm, where the spectral resonance position can be controlled by the pillar radius (SI, Figure S2). Superimposed on the transmission, we observe Fabry-Pérot interferences with a period of 0.2 nm, originating from the 500 μm thick LN substrate (SI, Figure S3). As the LN substrate is unaffected by the applied electric field, we focus the discussion on the filtered data after the Fabry-Pérot interference removal by Fourier transform filtering (SI, Figure S4).

We measure the modulation amplitude for the wavelength range of the laser while applying an 180 kHz AC voltage of 2 V_{pp}. Here, the photodiode signal is tracked by a lock-in amplifier referenced by the signal generator driving the open circuit. In order to determine the enhancement of the modulation as compared to an unstructured film, we define a modulation enhancement factor as the modulation amplitude of the metasurface divided by the modulation amplitude of an unpatterened reference area. The modulation enhancement (Figure 2a, right axis, solid orange line) shows a strong dependence on the wavelength of the laser, with an about 80× enhancement in the vicinity of the metasurface resonance. As the unstructured area shows no dependence on the wavelength (SI, Figure S5a, inset) and the electro-optic coefficient of LN is quasi-constant in the investigated wavelength range, this indicates that the modulation amplitude of the structured area is influenced by the transmission of the metasurface itself.

As the electro-optic transmission shift is small (SI, Figure S5b, inset), we postulate that the modulation amplitude corresponds to the derivative of the transmission. This is validated by the derivative (dashed cyan line) of the measured transmitted intensity of the metasurface (solid blue line) given

https://doi.org/10.1021/acsphotonics.1c00935
ACS Photonics XXXX, XXX, XXX−XXX

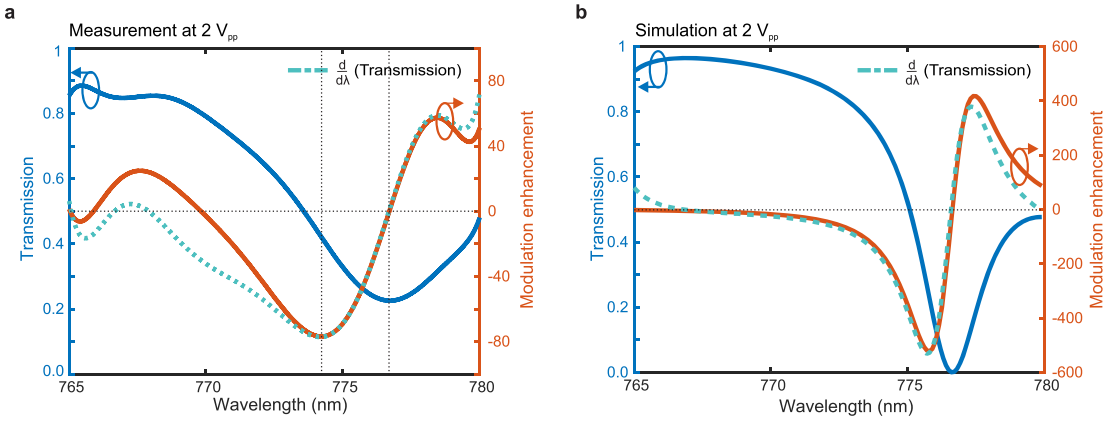

Figure 2. Wavelength dependence of the electro-optic response. (a) Measured transmission (blue) of a metasurface with radius 135 nm and period 500 nm, normalized by the transmission of an unstructured area. The orange line shows the modulation enhancement, defined as the modulation amplitude of the metasurface divided by the modulation amplitude of an unpatterned area, for an AC voltage of 2 V_{pp} and 180 kHz. The rescaled derivative of the transmitted signal (dashed cyan line) is shown as a guide to the eye. (b) Calculated transmission (blue) of a metasurface with radius 135 nm and period 500 nm, normalized by the transmission of an unstructured area. The orange line shows the modulation enhancement, defined as modulation amplitude of the metasurface divided by the modulation amplitude of an unpatterned area, for a voltage of 2 V_{pp}. The rescaled derivative of the transmitted signal (dashed cyan line) is shown as a guide to the eye.

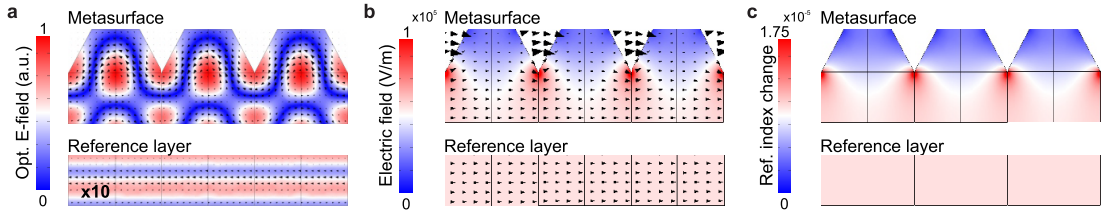

Figure 3. Optical field, electric field, and refractive index change distribution over the metasurface. (a) Optical field strength at the resonance wavelength in one unit cell of the metasurface (right) and reference layer (left) along a plane normal to the incident electric field. The arrows show the direction of the magnetic field. (b) Transversal cut with the distribution of the electric field norm created by the electrodes for the metasurface (up) and the reference layer (bottom). The arrowheads show the direction of the electric field. The cut is transversal to the LN surface, with the extraordinary axis along the vertical. **c** The change of refractive index induced by the electro-optic effect at 1 V in the metasurface unit cell (up) and the reference layer (bottom). In (a)−(c), three unit cells (width of 500 nm) of the metasurface/reference layer is shown. The change of refractive index is largest at the corners of the pillars as it is the position where the optical electric field (a) and the electric field (b) are largest.

in Figure 2a. We conclude that the transmission of the metasurface itself causes a dispersive electro-optic response in the modulation amplitude. This modulation response is therefore unique to every metasurface geometry, as we show for the other investigated metasurfaces (SI, Figure S6). Compared with the response of an unpatterned substrate, which is flat (SI, Figure S5), the modulation amplitude of the metasurface is enhanced by 2 orders of magnitude (-2.2×10^{-3}% on the metasurface compared to -0.026×10^{-3}% on the substrate) at 774.2 nm (dashed line in Figure 2a as guide to the eye). These modulation amplitudes correspond to an about 80× modulation enhancement at the metasurface compared to the substrate. It is worth noting that the negative sign of the enhancement factor or modulation amplitude does not imply less modulation (this would be true for factors between 0 and 1 such as at the resonance itself).

Subsequently, we investigate the origin of the electro-optic modulation enhancement with a finite element method (FEM) model. The transmission of the metasurface (Figure 2b, left axis, solid blue line), normalized to the reference layer (SI, Figure S5b, inset), was calculated using a model described in SI, S5 and Figure S7 and matches the measurements (Figure 2a). The quality factor of 272 of the simulated transmission resonance is higher than the measured one (129), which we attribute to fabrication imperfections. In the next step, we calculate the electric field distribution created by the gold electrodes using an extended model described in SI, Figure S10. Owing to the electrodes geometry, the electric field in the metasurface takes higher values in the edge unit cell and decreases uniformly toward the center of the metasurface (SI, Figure S10, insets). Using the simulated local electric field distribution in the central unit cell, we determine the local refractive index modification caused by the electro-optic effect. With the new value of the refractive index, we determine the modulation at 2 V_{pp} (Figure 2b, right axis, orange curve) using the method described in SI, section S8. Our simulation confirms the experimental result that the modulation of the metasurface has the highest enhancement (and absolute amplitude, Figure S5) at the steepest slope of the transmission spectrum. The deviation in magnitude between experimental and numerical enhancement factor is attributed to less pronounced edges between the pillars due to fabrication imperfections.

The optical field strength map in Figure 3a shows that the resonance is dominated by the electric dipole mode (SI, Figure S9). Further, we calculate the electric field from the electrodes with an FEM model (SI, Figure S10). We observe that the metasurface nanopatterning imprints a periodicity on the

https://doi.org/10.1021/acsphotonics.1c00935
ACS Photonics XXXX, XXX, XXX−XXX

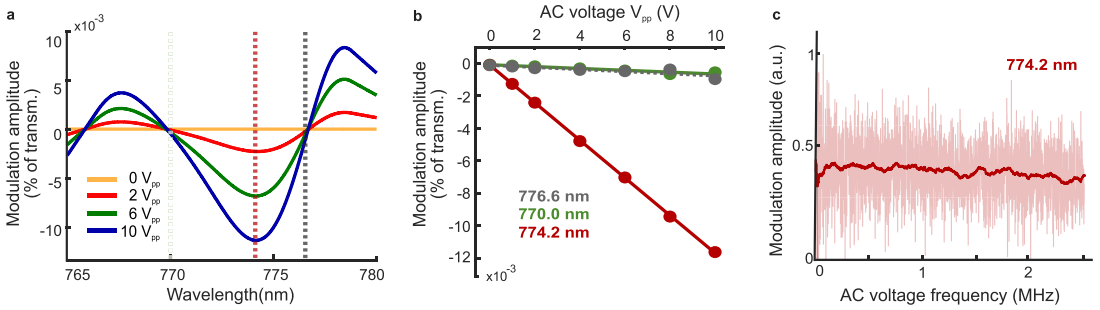

Figure 4. Performance of the electro-optic metasurface. (a) Dependence of the modulation amplitude on peak-to-peak AC voltage between 0 V_{pp} (no modulation) and 10 V_{pp} (strong modulation) with 180 kHz driving frequency. The dashed colored lines are the same as in Figure 2a and indicate the position of the cross sections in (b). (b) Modulation amplitude upon application of an increasing AC voltage at 770 (green line), 774.2 (red line), and 776.6 nm (gray, dashed line). The peak-to-peak voltage is indicated on the horizontal axis. The dots are measured data at 180 kHz driving frequency, while the solid lines are linear fits. (c) Measured frequency dependence of the modulation amplitude between 1 kHz and 2.5 MHz at 774.2 nm. The solid red line is the smoothed data.

electric field (Figure 3b, top), whereas the electric field in the reference layer is uniform (Figure 3b, bottom). As expected for a dielectric material, the electric field strength is larger in the surrounding air (Figure S11). As air does not exhibit an electro-optic response, the electric field in air is neglected in Figure 3b due to better visibility. Comparing Figure 3a and b, a clear overlap of the electric hotspots with the optical field at the corners of the metasurface is visible. This is relevant as the electric field hotspots are also the locations of biggest change in refractive index (Figure 3c), which will eventually change the transmission behavior of the metasurface. On average, the refractive index change has similar values for the metasurface and the reference layer. However, around the resonance this change leads to a much stronger effect on the transmission and the electro-optic modulation. Having investigated the microscopic origin of the modulation, the next section will be dedicated to the evaluation of the performance of the device and the characterization of the linear electro-optic effect.

Conveniently, the dispersive electro-optic modulation response offers two approaches for changing the electro-optic modulation strength: the operating wavelength and the driving voltage. The modulation amplitude changes the most at the extrema of the derivative of the transmission, as shown in Figure 4a for different V_{pp} values. Consequently, the electro-optic modulation barely changes at the extreme values of the transmission itself (green and gray dashed line), even upon application of higher voltages. To investigate the influence of the electric field on the modulation amplitude, we fix the laser at chosen wavelengths (Figure 4b): off-resonance (770 nm), at the steepest drop of the transmitted intensity (774.2 nm) and at the resonance (776.6 nm). Upon increasing V_{pp}, we observe that the modulation amplitude scales linearly with the applied voltage and reaches 0.01% at 10 V_{pp}. This strongly validates the dominance of the linear electro-optic effect for the modulation of the metasurfaces and is further confirmed by the independence of the modulation amplitude on the laser power, that excludes a thermo-optic effect (SI, Figure S12). The electro-optic modulation can be detected already for voltages below 1 V_{pp}, indicating the practical impact of this device for low-power consumption applications. The different slopes in Figure 4b reveal that the modulation at 774.2 nm scales 1 order of magnitude higher to the applied voltage than the off-resonant/on-resonance case, which further confirms the dispersive electro-optic behavior.

The bandwidth of the modulation, which defines the driving frequencies of the device, is in the MHz region. We can operate in a frequency range from a few Hz (SI, Figure S12) up to the MHz-region, with a flat response to the driving frequency from 1 kHz up to 2.5 MHz (Figure 4c), limited only by the electrical scheme. Based on LN properties, our device should be operational at modulation frequencies up to the GHz regime.[23,34] However, the modulation response in the MHz-frequency range already supports the dominant linear electro-optic effect since other modulating effects (e.g., thermal) exhibit lower characteristic time scales.[35]

In conclusion, we demonstrate an all-dielectric LN metasurface in the visible with a resonance that can be actively and continuously tuned based on the linear electro-optic effect. This metasurface shows a versatile way of realizing small, low-loss, and tunable optical devices operating in the visible to near-infrared range and offering fast modulation. We show that the electro-optic modulation amplitude is wavelength-dependent and enhanced through the optical resonance of the metasurface by a factor of 80 in magnitude compared to an unstructured film, which corresponds to a two orders of magnitude enhancement. The agreement with the simulations supports the experimental findings and their interpretations. We achieve a frequency-independent modulation amplitude between 10 Hz and 2.5 MHz for voltages below 1 V, which allows driving our device by commercial microcontrollers. The modulation amplitude of 0.01% in our proof-of-concept work is rather small for practical applications. There are several strategies on how to boost the modulation amplitude in the future. First of all, a sharper resonance with a higher *Q*-factor would increase the modulation amplitude. Promising resonance types could be, for example, bound states in the continuum or Fano resonances.[36−38] Enhancing the overlap of the electric with the optical field would improve the modulation, which could also further be optimized by an advanced fabrication to obtain sharper structures. Electrodes on top and on the bottom of the metasurface may be preferable, but such a configuration is a challenge with the current available LN substrate platforms. More diverse applications could be reached by single pixel modulation,[5] which would require further improvements on the electrode designs. Another interesting approach is to combine LN with other all-dielectric materials, for example, silicon for hybrid electro-optic platforms as theoretically predicted.[39]

https://doi.org/10.1021/acsphotonics.1c00935
ACS Photonics XXXX, XXX, XXX−XXX

Future work includes an extension of the setup to investigations up to the GHz-regime and an optimized design for better electric and optic field overlap or higher Q-factor resonances. This could lead to a stronger enhancement of the electro-optic modulation amplitude. However, our proof-of-concept work already gives the experimental demonstration on how the electro-optic modulation amplitude is enhanced at a metasurface resonance and is to date the fastest and strongest electro-optically modulated metasurface. With further improvements, tunable lenses and color displays are within reach. The fast tuning properties of our LN device could lead to advances in beam steering and ultimately push free-space data processing to the next level.

METHODS

Metasurface Fabrication. The metasurfaces presented in this work were fabricated at the cleanroom facilities of the Binnig and Rohrer Nanotechnology Center (BRNC). The sample was fabricated on a commercially available x-cut lithium niobate-on-insulator thin film chip with a top-down approach using reactive ion etching. The gold electrodes were deposited using a lift-off process after electron-beam evaporation. A detailed fabrication report can be found in the Supporting Information.

Simulations. All the presented simulations were performed using FEM models in COMSOL Multiphysics 5.5, which are described in detail in the Supporting Information. We modeled the origin of the rapid oscillations in Figure 1e by comparing two 2D FEM models, one including the full 500 μm LN wafer and one including a semi-infinite LN wafer (SI, section S3). We calculate the transmission of a metasurface and of the reference using a 3D model shown in section S6, which takes into account the particular geometry of our sample. This method is based on previous works, described in detail elsewhere.[40] To account for the electro-optic effect, we combine the method shown in section S6 with a previous step using the electrostatic module of COMSOL Multiphysics (SI, section S8). In this step, we calculate the electric field created by two gold electrodes in a full slice along the extraordinary axis. Using this result, we update the value of the refractive index with the electro-optic contribution and use the new refractive index value to run the model in section S6.

ASSOCIATED CONTENT

Supporting Information

The Supporting Information is available free of charge at https://pubs.acs.org/doi/10.1021/acsphotonics.1c00935.

Detailed description of fabrication, simulation, and experimental setup. Investigation of other metasurfaces with different resonances and study on laser polarization dependence and laser power dependence. Multipole expansion of the resonance, investigation of Fabry–Perot resonances, and simulations on the electric field distribution are presented. Modulation at low frequencies is shown (PDF)

AUTHOR INFORMATION

Corresponding Author

Helena Weigand − *ETH Zurich, Department of Physics, Institute for Quantum Electronics, Optical Nanomaterial Group, 8093 Zurich, Switzerland;* orcid.org/0000-0003-0558-5899; Email: hweigand@phys.ethz.ch

Authors

Viola V. Vogler-Neuling − *ETH Zurich, Department of Physics, Institute for Quantum Electronics, Optical Nanomaterial Group, 8093 Zurich, Switzerland*

Marc Reig Escalé − *ETH Zurich, Department of Physics, Institute for Quantum Electronics, Optical Nanomaterial Group, 8093 Zurich, Switzerland*

David Pohl − *ETH Zurich, Department of Physics, Institute for Quantum Electronics, Optical Nanomaterial Group, 8093 Zurich, Switzerland*

Felix U. Richter − *ETH Zurich, Department of Physics, Institute for Quantum Electronics, Optical Nanomaterial Group, 8093 Zurich, Switzerland*

Artemios Karvounis − *ETH Zurich, Department of Physics, Institute for Quantum Electronics, Optical Nanomaterial Group, 8093 Zurich, Switzerland*

Flavia Timpu − *ETH Zurich, Department of Physics, Institute for Quantum Electronics, Optical Nanomaterial Group, 8093 Zurich, Switzerland;* orcid.org/0000-0002-0951-4070

Rachel Grange − *ETH Zurich, Department of Physics, Institute for Quantum Electronics, Optical Nanomaterial Group, 8093 Zurich, Switzerland;* orcid.org/0000-0001-7469-9756

Complete contact information is available at: https://pubs.acs.org/10.1021/acsphotonics.1c00935

Author Contributions

†These authors contributed equally to this work.

Notes

The authors declare no competing financial interest.

R.G., F.T., H.W., and V.V.-N. designed the experiment. V.V.-N., H.W., and F.R. built the setup. H.W., V.V.-N., and F.T. conducted the experiments. M.R.E., H.W., and D.P. fabricated the device. H.W. analyzed the data with contributions from F.T. and V.V.-N. F.T. did the simulations. H.W., F.T., and V.V.-N. wrote the manuscript with contributions from M.R.E., D.P., F.R., A.K., and R.G.

ACKNOWLEDGMENTS

We acknowledge support for nanofabrication from FIRST of ETH Zurich. We thank the Cleanroom Operations Team of the Binnig and Rohrer Nanotechnology Center (BRNC) for their help and support. This work was supported by the European Union's Horizon 2020 Research and Innovation Program from the European Research Council under Grant Agreement No. 714837 (Chi2-nano-oxides) and MCSA Grant No. 801459 (FP-RESOMUS). Furthermore, it was supported by the Swiss National Science Foundation with Grant Nos. 179099 and 150609 and through the NCCR MUST. F.T. and H.W. acknowledge financial support from the Physics Department at ETH Zurich.

REFERENCES

(1) Minovich, A. E.; Miroshnichenko, A. E.; Bykov, A. Y.; Murzina, T. V.; Neshev, D. N.; Kivshar, Y. S. Functional and Nonlinear Optical Metasurfaces. *Laser Photonics Rev.* **2015**, *9* (2), 195−213.

(2) Lalanne, P.; Chavel, P. Metalenses at Visible Wavelengths: Past, Present, Perspectives. *Laser Photonics Rev.* **2017**, *11* (3), 1600295.

(3) Chen, W. T.; Zhu, A. Y.; Capasso, F. Flat Optics with Dispersion-Engineered Metasurfaces. *Nat. Rev. Mater.* **2020**, *5* (8), 604−620.

(4) Neshev, D.; Aharonovich, I. Optical Metasurfaces: New Generation Building Blocks for Multi-Functional Optics. *Light: Sci. Appl.* **2018**, *7* (1), 58.
(5) Shaltout, A. M.; Shalaev, V. M.; Brongersma, M. L. Spatiotemporal Light Control with Active Metasurfaces. *Science (Washington, DC, U. S.)* **2019**, *364* (6441), No. eaat3100.
(6) Horie, Y.; Arbabi, A.; Arbabi, E.; Kamali, S. M.; Faraon, A. High-Speed, Phase-Dominant Spatial Light Modulation with Silicon-Based Active Resonant Antennas. *ACS Photonics* **2018**, *5* (5), 1711−1717.
(7) Celebrano, M.; Rocco, D.; Gandolfi, M.; Zilli, A.; Rusconi, F.; Tognazzi, A.; Mazzanti, A.; Ghirardini, L.; Pogna, E. A. A.; Carletti, L.; Baratto, C.; Marino, G.; Gigli, C.; Biagioni, P.; Duò, L.; Cerullo, G.; Leo, G.; Della Valle, G.; Finazzi, M.; De Angelis, C. Optical Tuning of Dielectric Nanoantennas for Thermo-Optically Reconfigurable Nonlinear Metasurfaces. *Opt. Lett.* **2021**, *46* (10), 2453−2456.
(8) Liu, S.; Vabishchevich, P. P.; Vaskin, A.; Reno, J. L.; Keeler, G. A.; Sinclair, M. B.; Staude, I.; Brener, I. An All-Dielectric Metasurface as a Broadband Optical Frequency Mixer. *Nat. Commun.* **2018**, *9* (1), 2507.
(9) Huang, Z.; Lu, H.; Xiong, H.; Li, Y.; Chen, H.; Qiu, W.; Guan, H.; Dong, J.; Zhu, W.; Yu, J.; Luo, Y.; Zhang, J.; Chen, Z. Fano Resonance on Nanostructured Lithium Niobate for Highly Efficient and Tunable Second Harmonic Generation. *Nanomaterials* **2019**, *9* (1), 69.
(10) Chang, L.; Li, Y.; Volet, N.; Wang, L.; Peters, J.; Bowers, J. E. Thin Film Wavelength Converters for Photonic Integrated Circuits. *Optica* **2016**, *3* (5), 531.
(11) Ee, H.-S.; Agarwal, R. Tunable Metasurface and Flat Optical Zoom Lens on a Stretchable Substrate. *Nano Lett.* **2016**, *16* (4), 2818−2823.
(12) Kamali, S. M.; Arbabi, E.; Arbabi, A.; Horie, Y.; Faraon, A. Highly Tunable Elastic Dielectric Metasurface Lenses. *Laser Photonics Rev.* **2016**, *10* (6), 1002−1008.
(13) Arbabi, E.; Arbabi, A.; Kamali, S. M.; Horie, Y.; Faraji-Dana, M. S.; Faraon, A. MEMS-Tunable Dielectric Metasurface Lens. *Nat. Commun.* **2018**, *9* (1), na DOI: 10.1038/s41467-018-03155-6.
(14) Sautter, J.; Staude, I.; Decker, M.; Rusak, E.; Neshev, D. N.; Brener, I.; Kivshar, Y. S. Active Tuning of All-Dielectric Metasurfaces. *ACS Nano* **2015**, *9* (4), 4308−4315.
(15) Huang, Y. W.; Lee, H. W. H.; Sokhoyan, R.; Pala, R. A.; Thyagarajan, K.; Han, S.; Tsai, D. P.; Atwater, H. A. Gate-Tunable Conducting Oxide Metasurfaces. *Nano Lett.* **2016**, *16* (9), 5319−5325.
(16) Park, J.; Kang, J. H.; Kim, S. J.; Liu, X.; Brongersma, M. L. Dynamic Reflection Phase and Polarization Control in Metasurfaces. *Nano Lett.* **2017**, *17* (1), 407−413.
(17) Karvounis, A.; Vogler-Neuling, V. V.; Richter, F. U.; Dénervaud, E.; Timofeeva, M.; Grange, R. Electro-Optic Metasurfaces Based on Barium Titanate Nanoparticle Films. *Adv. Opt. Mater.* **2020**, *8* (17), 2000623.
(18) Hail, C. U.; Michel, A.-K. U.; Poulikakos, D.; Eghlidi, H. Optical Metasurfaces: Evolving from Passive to Adaptive. *Adv. Opt. Mater.* **2019**, *7* (14), 1801786.
(19) Wang, Q.; Rogers, E. T. F.; Gholipour, B.; Wang, C. M.; Yuan, G.; Teng, J.; Zheludev, N. I. Optically Reconfigurable Metasurfaces and Photonic Devices Based on Phase Change Materials. *Nat. Photonics* **2016**, *10* (1), 60−65.
(20) He, Q.; Sun, S.; Zhou, L. Tunable/Reconfigurable Metasurfaces: Physics and Applications. *Research* **2019**, *2019*, 1−16.
(21) Gaborit, G.; Dahdah, J.; Lecoche, F.; Jarrige, P.; Gaeremynck, Y.; Duraz, E.; Duvillaret, L. A Nonperturbative Electrooptic Sensor for in Situ Electric Discharge Characterization. *IEEE Trans. Plasma Sci.* **2013**, *41* (10), 2851−2857.
(22) Honardoost, A.; Abdelsalam, K.; Fathpour, S. Rejuvenating a Versatile Photonic Material: Thin-Film Lithium Niobate. *Laser Photonics Rev.* **2020**, *14* (9), 2000088.
(23) Wooten, E. L.; Kissa, K. M.; Yi-Yan, A.; Murphy, E. J.; Lafaw, D. A.; Hallemeier, P. F.; Maack, D.; Attanasio, D. V.; Fritz, D. J.; McBrien, G. J.; Bossi, D. E. A Review of Lithium Niobate Modulators for Fiber-Optic Communications Systems. *IEEE J. Sel. Top. Quantum Electron.* **2000**, *6* (1), 69−82.
(24) Wang, C.; Zhang, M.; Chen, X.; Bertrand, M.; Shams-Ansari, A.; Chandrasekhar, S.; Winzer, P.; Lončar, M. Integrated Lithium Niobate Electro-Optic Modulators Operating at CMOS-Compatible Voltages. *Nature* **2018**, *562* (7725), 101−104.
(25) Palik, E. D. Lithium Niobate. *Handbook of Optical Constants of Solids I*; Academic Press, 1997; pp 695−702, DOI: 10.1007/978-3-540-70766-0.
(26) Wang, C.; Zhang, M.; Stern, B.; Lipson, M.; Lončar, M. Nanophotonic Lithium Niobate Electro-Optic Modulators. *Opt. Express* **2018**, *26* (2), 1547−1555.
(27) Fedotova, A.; Younesi, M.; Sautter, J.; Vaskin, A.; Löchner, F. J. F.; Steinert, M.; Geiss, R.; Pertsch, T.; Staude, I.; Setzpfandt, F. Second-Harmonic Generation in Resonant Nonlinear Metasurfaces Based on Lithium Niobate. *Nano Lett.* **2020**, *20* (12), 8608−8614.
(28) Carletti, L.; Zilli, A.; Moia, F.; Toma, A.; Finazzi, M.; De Angelis, C.; Neshev, D. N.; Celebrano, M. Steering and Encoding the Polarization of the Second Harmonic in the Visible with a Monolithic LiNbO3Metasurface. *ACS Photonics* **2021**, *8* (3), 731−737.
(29) Ma, J.; Xie, F.; Chen, W.; Chen, J.; Wu, W.; Liu, W.; Chen, Y.; Cai, W.; Ren, M.; Xu, J. Nonlinear Lithium Niobate Metasurfaces for Second Harmonic Generation. *Laser Photonics Rev.* **2021**, *15* (5), 2000521.
(30) Santiago-Cruz, T.; Fedotova, A.; Sultanov, V.; Weissflog, M. A.; Arslan, D.; Younesi, M.; Pertsch, T.; Staude, I.; Setzpfandt, F.; Chekhova, M. Photon Pairs from Resonant Metasurfaces. *Nano Lett.* **2021**, *21* (10), 4423−4429.
(31) Gao, B.; Ren, M.; Wu, W.; Cai, W.; Xu, J. Electro-Optic Lithium Niobate Metasurfaces. *Sci. China: Phys., Mech. Astron.* **2021**, *64* (4), 240362.
(32) Weis, R. S.; Gaylord, T. K. Lithium Niobate: Summary of Physical Properties and Crystal Structure. *Appl. Phys. A: Solids Surf.* **1985**, *37* (4), 191−203.
(33) Gao, B. F.; Ren, M. X.; Wu, W.; Cai, W.; Xu, J. J. Electro-Optic Lithium Niobate Metasurfaces. *Sci. China: Phys., Mech. Astron.* **2021**, *64* (4), na DOI: 10.1007/s11433-021-1668-y.
(34) Pohl, D.; Messner, A.; Kaufmann, F.; Escalé, M. R.; Holzer, J.; Leuthold, J.; Grange, R. 100-GBd Waveguide Bragg Grating Modulator in Thin-Film Lithium Niobate. *IEEE Photonics Technol. Lett.* **2021**, *33* (2), 85−88.
(35) Shalaginov, M. Y.; Campbell, S. D.; An, S.; Zhang, Y.; Ríos, C.; Whiting, E. B.; Wu, Y.; Kang, L.; Zheng, B.; Fowler, C.; Zhang, H.; Werner, D. H.; Hu, J.; Gu, T. Design for Quality: Reconfigurable Flat Optics Based on Active Metasurfaces. *Nanophotonics* **2020**, *9* (11), 3505−3534.
(36) Kuznetsov, A. I.; Miroshnichenko, A. E.; Brongersma, M. L.; Kivshar, Y. S.; Lukyanchuk, B. Optically Resonant Dielectric Nanostructures. *Science* **2016**, *354* (6314), aag2472.
(37) Koshelev, K.; Bogdanov, A.; Kivshar, Y. Boosting Second-Harmonic Generation in Nonlinear Metasurfaces with Bound States in the Continuum. *Conference on Lasers and Electro-Optics*; OSA Technical Digest; Optical Society of America: San Jose, CA, 2019; p JTh2A.117, DOI: 10.1364/CLEO_AT.2019.JTh2A.117.
(38) Yang, Y.; Wang, W.; Boulesbaa, A.; Kravchenko, I. I.; Briggs, D. P.; Puretzky, A.; Geohegan, D.; Valentine, J. Nonlinear Fano-Resonant Dielectric Metasurfaces. *Nano Lett.* **2015**, *15* (11), 7388−7393.
(39) Barton, D.; Lawrence, M.; Dionne, J. Wavefront Shaping and Modulation with Resonant Electro-Optic Phase Gradient Metasurfaces. *Appl. Phys. Lett.* **2021**, *118* (7), 071104.
(40) Timpu, F.; Reig Escalé, M.; Timofeeva, M.; Strkalj, N.; Trassin, M.; Fiebig, M.; Grange, R. Enhanced Nonlinear Yield from Barium Titanate Metasurface Down to the Near Ultraviolet. *Adv. Opt. Mater.* **2019**, *7* (22), 1900936.

https://doi.org/10.1021/acsphotonics.1c00935
ACS Photonics XXXX, XXX, XXX−XXX